PROCEDURE BASED ON COMPOSITE FEM TECHNOLOGY FOR THE RESOLUTION OF CONCRETE FRAMED STRUCTURES WITH MASONRY IN-FILLS - COMPARISON WITH MEXICAN BUILDING CODE.

Cuauhtemoc Escudero [1] [2] (cuauhtemoc@cimne.upc.edu),
Sergio Oller [1] [2] (sergio.oller@upc.edu),
Xavier Martinez [2] [3] (xmartinez@cimne.upc.edu),
Alex Barbat [1] [2] (alex.barbat@upc.edu).

ABSTRACT

The construction of confined masonry buildings have become a good choice to meet the housing needs of low income families in big cities. Despite this, current building codes for such constructions, allows the use of highly simplified analysis techniques, that have hardly changed in the last 40 years.

This paper is based on the numerical simulation, and emerges as the need to combine and improve existing technologies in the field of FEM (**F**inite **E**lement **M**ethod) analysis for composite materials, to assess the overall structural behavior of reinforced concrete structures with masonry in-fills, and consequently, to support the derivation of rational rules for analysis and design purposes. So, through the use of a simple yet powerful shell FE (**F**inite **E**lement), the state-of-the-art theories of mixtures to analyze composite materials, a computational tool to generate the volume fraction of composites, and a Mexican building code, this paper pretends to be a guidance to numerically reproduce the overall behavior of confined masonry structures.

Keywords: Laminated element, Composite materials, large reinforced concrete (RC) structures, mechanical plane, Masonry structures, Mexican building code

INTRODUCTION

Confined masonry construction was introduced in Mexico City, Mexico, in the 1940's to control the wall cracking caused by large differential settlements under

[1]Departamento de Resistencia de Materiales y Estructuras en la Ingeniería, ETSECCPB, Technical University of Catalonia, Spain.

[2]Centre Internacional de Metodes Numerics en Enginyeria (CIMNE), Gran Capitá s/n, 08034 Barcelona, Spain

[3]Departamento de Ciencia e Ingeniería Náutica, FBN, Technical University of Catalonia, Pla de Palau 18, 08003 Barcelona, Spain

soft soil conditions. Several years later, this system became popular in other areas of highest seismic hazard due to its excellent earthquake performance (Meli and Alcocer 2004), but was until early 60s when the proper study of confined masonry started in the country, when Esteva (Esteva 1961; Esteva 1966; Esteva 1963) tested masonry walls confined with reinforced concrete. Later on, several studies were made at the time, like the ones made by Meli *et al.* (Meli et al. 1968), Meli and Salgado (Meli and Salgado 1969), Madinaveitia and Rodríguez (Madinaveitia and Rodríguez 1970), Turkstra (Turkstra 1970), Meli and Reyes (Meli and Reyes 1971), Madinaveitia (Madinaveitia 1971), Meli and Hernández (Meli and Hernández 1971; Meli and Hernández 1975), being the bases upon Hernández in 1975 (Hernández 1975) provided design and construction recommendations for structures made out of masonry bearing walls. Thus, in 1977 the first Mexican code for design and construction of masonry structures was established, where, for design purposes, a simplified use of mechanical of materials theories is used, which led to model confined masonry building subjected to ground shaking, mainly:

a. As a **truss** (Brzev 2007), where masonry walls act as diagonal struts subjected to compression, whereas the reinforced concrete confining members act in tension/compression, depending on the lateral earthquake forces.
b. As a **frame** (Fundación 1999), where confined masonry walls are modeled using an equivalent column, it is assumed the beams have infinite stiffness, and diagonal struts are used to model the slabs.

In both cases, the analogy made are highly simplistic and lack in accuracy. Researching work has also been extended to the numerical field applying the finite element method. The majority of the proposed modeling strategies, in order to study the mechanical behavior of masonry has been identified by Lourenço (Lourenço 1996) and Rots (Rots 1997), and can be classified in two categories:

- **Micro-modeling, or two-phase material models**: where the components are considered separately to account for the different inelastic behavior, and the interaction between them. Analysis within this category are computationally quite expensive to use due to several reasons, such as, the great number of degrees of freedom involved, they require more input data, and their failure criterion has a complicated form because of the brick-mortar interaction. On the other hand, the constitutive equations of the components have normally a simple form, and they are suitable for the study of local behavior of masonry. This modeling strategy is categorized into

    a. *Detailed micro-modeling* where units and mortars are represented as continuum, with the unit/mortar interfaces modeled using discontinuous interfaces elements as potential cracks, slip and crushing planes.

b. *Simplified micro-modeling* through the adoption of *geometrically expanded* masonry units with a single average interface representing the mortar and the two mortar/unit interfaces. This models requires the material model of the expanded unit and masonry joints.

- **Macro-modeling or one-phase material models**: treat masonry as an ideal homogeneous single material with constitutive models that differ from those of the components (mortar and bricks). The constitutive models of this category are more efficient for a practice-oriented analysis due to the reduced calculation time and memory requirements, as well as due to the user-friendly mesh generation. The resulting material is regarded as an anisotropic composite and a relation is established between average masonry strains and average masonry stresses. Such material must reproduce an orthotropic behavior as well as different tensile and compressive strengths along the material axes and different inelastic behavior for each material axis, which leads in more complicated constitutive equations.

Current theories that allow the use of two-dimensional FE to model three-dimensional structures with composite materials, yet powerful, lack the necessary simplicity for their application in complex structures, where a large amount of FE are required to obtain a good approximation of the result. Thus, simpler and more efficient techniques are required for modeling three-dimensional laminated structures.

The main objective of this work, is to develop an efficient methodology, and to be able of numerically reproduce the behavior of an entire masonry structure, to subsequently, find reliable estimates of the non-linear response which leads to fully understand the failure mechanisms and assess its safety.

In order to achieve this objective, the state of the art for shell elements and for rules of mixtures for composite materials has been reviewed. Also the code regulations regarding the analysis and design of masonry buildings have been reviewed, to compare the obtained results with the proposed analysis scheme.

Finally, the theoretical principles used will be defined and applied to assemble a robust numerical tool capable of predicting the behavior of *real life* structures from linear elastic stage, through cracking and degradation until complete loss of strength.

The paper is organized as follows. In section 2 is briefly described the used FE formulation for a shell finite element that reproduces in-plane (membrane) and out-of-plane (bending) non-linear behavior, also is described the used constitutive formulation for simple materials and for composite materials. Section 3 describes the methodology to determine the information related to the simple and composite materials, the procedure to mechanically generate the volume fraction for the composite materials, and a description of the followed computational strategy. Finally in section 4 a numerical tests is presented and compared with the Mexican in force Building code.

The proposed approach is a general purpose one to treat large-scale reinforced concrete structures with masonry in-fills. The use of the Mexican Code was merely to have a base to compare the obtained results in terms of initial stiffness and total shear strength.

FINTE ELEMENT FORMULATION

Simulation of large multi-layered structures with many plies can be unaffordable with three-dimensional analyses because of the excessive computational cost, especially for non-linear materials. In addition, the discretization of very thin layers can lead to highly distorted elements carrying numerical issues, hence, reduced models using multilayer shell elements arise as an affordable solution (Eijo 2014). In this section is carried out a brief description of the shell element used along this work, which besides its reliability, one key aspect which led to select it was the computational resources required for its implementation in a FE code.

Shell element model

One of the most popular approaches in the FE analysis of shells is to use an assemblage of flat triangular elements as an approximation to the curved surface, in addition, such FE can be obtained by combining a membrane and a plate bending element (Khosravi et al. 2007).

There are several triangular plate bending elements to select and combine with membrane elements, next is carried out a brief description of the membrane and bending which have been selected due to their reliability (Batoz 1982; Felippa 2003).

Membrane element

A membrane element without including a in-plane rotation degree (*drilling rotation*) leads to in-plane rotation singularity (Hughes and Brezzi 1989). Successful attempts at developing membrane elements with drilling degree of freedom are due to the work by Allman (Allman 1984) and later Felippa (Bergan and Felippa 1985) developed an **OPT**imal membrane element with drilling degree of freedom.

The degrees of freedom of the OPT membrane element are collectable in the nodal displacement vector as

$$\boldsymbol{d}_m = \{u_1\ v_1\ \theta_{z1}\ u_2\ v_2\ \theta_{z2}\ u_3\ v_3\ \theta_{z3}\ \}^{\mathrm{T}} \tag{1}$$

The fundamental element stiffness decomposition of the two-stage direct fabrication method is

$$\mathbf{K}_m = \mathbf{K}_{mb} + \mathbf{K}_{mh} \tag{2}$$

where $\mathbf{K}_{mb}$ is the basic stiffness, which take care of the consistency, and $\mathbf{K}_{mh}$ is the high order stiffness, which takes care of stability (rank sufficiency) and accuracy. The final form of $\mathbf{K}_m$ is a template with 11 free parameters, leading to

$$\mathbf{K}_m^{(\alpha_b,\beta_0,\ldots,\beta_9)} = \frac{1}{\mathrm{V}}\mathbf{L}\mathbf{D}_m\mathbf{L}^{\mathrm{T}} + \int_\Omega \mathbf{B}_m^{\mathrm{T}}\mathbf{D}_m\mathbf{B}_m\, dv \tag{3}$$

For a full reference of the geometry and the computational implementation of the OPT element reader may consult reference (Felippa 2003) where an extensive study of high-performance elements using an ANDES (**A**sumed **N**atural **DE**viatoric **S**train) template is presented.

Bending element

Batoz (Batoz 1982) studied several triangular Kirchhoff plate bending elements and showed that **D**iscrete **K**irchhoff **T**riangle (DKT) (Batoz et al. 1980) is the most reliable triangular element for the analysis of thin plates, d.o.f for such element can be presented in a vector as

$$\boldsymbol{d}_b = \{w_1\ \theta_{x1}\ \theta_{y1}\ w_1\ \theta_{x2}\ \theta_{y2}\ w_1\ \theta_{x3}\ \theta_{y3}\}^{\mathrm{T}} \tag{4}$$

where the evaluation of the stiffness matrix follows the standard procedures of the finite elements methods, this is

$$\mathbf{K}_b = \int_\Omega \mathbf{B}_b^{\mathrm{T}} \mathbf{D}_b \mathbf{B}_b \, dA = 2A \int_0^1 \int_0^{1-\zeta_3} \mathbf{B}_b^{\mathrm{T}} \mathbf{D}_b \mathbf{B}_b \, d\zeta_2 d\zeta_3 \tag{5}$$

For a full description of the DKT element and for the numeric implementation reader may consult reference (Batoz et al. 1980).

In this work, it will be used the DKT element combined with the enhancement to the plate element proposed by Escudero (Escudero 2015; Escudero et al. 2016), where in the integration along the thickness of the element is used an ESL (**E**quivalent **S**ingle **L**ayer) description which takes into account the evolution of the eccentricity of geometric and mechanical planes. This makes it suitable for modeling the bending damage of shell structures at a *low* computational cost, since there is no need of additional degrees of freedom that the ones listed in equation 4.

Constitutive formulation

In this section a brief description of the expected bending degradation is carried out, focusing on the evaluation of the secant constitutive tensor $\mathbf{D}^{sec}$, which is required to reproduce the bending degradation that arises when some layers within a laminated plate are beyond the elastic threshold and others are not.

Concrete

Concrete is a composite material, since it is produced of a granular material (*aggregate*) embedded in a hard matrix of material (*cement*), however, it is a common practice to represent its behavior using a macro-model scheme for a simple *quasi-brittle geo-material*, even though its high non-linear performance is achieved due formation of micro-cracks and slipping among its aggregate particles (Oller 1998).

Large interest given to mechanical properties of concrete comes from its wide application range to the construction field, which has led to several authors to develop constitutive models to represent its mechanical behavior (Bazant and

Pijaudier-Cabot 1989; Hillerborg et al. 1976; Rots and De Borst 1987). However, it was not until early eighty when models (Chaboche 1988a; Chaboche 1988b; Ju 1989; Lemaitre 1985; Oliver et al. 1990; Simo and Ju 1987; Simo and Ju 1989) based upon the CMD (**C**ontinuum **D**amage **M**echanics) were applied to model concrete materials.

Two-scalar damage models Among the different possibilities the CDM offer, the simplest is the one referring to isotropic damage models where the non-linear behavior is monitored through a single internal scalar variable d called *damage* or *degradation*. The meaning of the internal variable d is the measurement of the loss of stiffness in the material, and it ranges from 0 to 1, being 0 an undamaged material and 1 for a fully degraded one (Oliver et al. 1990).
Another approach highly extended to model the opening and closing of cracks due cyclic loads in geomaterials is the one proposed by Faria *et al* in (Faria et al. 1998), where two scalar damage variables d^+ and d^- are introduced as internal variables, so it is possible to distinguish among the damage produced by tensile stresses (*cracking*) and the damage produced due compressive stresses (*crushing*). The nature of the scheme proposed by Faria *et al* makes it more convenient for seismic analysis purposes.
From the definition of the elastic secant constitutive tensor, it can be evaluated for this scheme as (Faria et al. 1998):

$$\mathbf{D}^{sec} = \frac{\partial \boldsymbol{\sigma}}{\partial \boldsymbol{\varepsilon}} = (1 - d^+)\frac{\partial^2 \Psi_0^+}{\partial \boldsymbol{\varepsilon}^e \otimes \partial \boldsymbol{\varepsilon}^e} + (1 - d^-)\frac{\partial^2 \Psi_0^-}{\partial \boldsymbol{\varepsilon}^e \otimes \partial \boldsymbol{\varepsilon}^e} \tag{6}$$

where

$$\boldsymbol{\sigma} = \mathbf{D}^{sec} \,:\, \boldsymbol{\varepsilon} \tag{7}$$

The use of two internal variables to reproduce the damage is an advantage in terms of the constitutive analysis, on the other hand, it becomes cumbersome while trying to establish one single parameter that defines the degradation of the material. This it can only be achieved with a equivalent damage index (Paredes et al. 2011) (eq. 13).
In this work the damage model to represent the behavior of geomaterials will be carried out using the scheme presented by Paredes (Paredes 2013), which conceptually is based on the scheme proposed by Faria, consisting in a two-scalar damage model.

Masonry

Depending on the accuracy and the simplicity desired, masonry can be modeled using:

- **Detailed Micro-Modeling**: Units and mortar in the joints are represented by continuum elements whereas the unit-mortar interface is represented by discontinuous elements.

- **Simplified Micro-Modeling**: Expanded units are represented by continuum elements whereas the behavior of the mortar joints and unit-mortar interface is lumped in discontinuous elements.
- **Macro-Modeling**: Units, mortar, and unit-mortar interface are bonded in the continuum.
- **Homogenized Modeling**: This strategy is placed midway between micro-modeling and macro-modeling, since it consists in obtaining macro-constitutive laws starting from the micro-constitutive law of the constituents and the internal geometry of the masonry.

Advantages and disadvantages of each approach are discussed in (Lourenco et al. 2007; Lourenço 1996; Pelà 2009). This work uses a *Macro-Modeling* approach, combininig the damage model proposed by Paredes (Paredes 2013) with the orthotropic yield criterion proposed by Oller *et al* (Oller et al. 2003). The macro-modeling scheme will be used because it is more practice oriented, due to the reduced time and memory requirements, as well as for the implied user-friendly mesh generation. Also because it provides the best compromise between accuracy and efficiency.

Orthotropic yield criterion The objective of the approach proposed by Oller *et al.* (Oller et al. 2003) is to adjust an arbitrary isotropic yield criterion to the behavior of an anisotropic material. Is very convenient to apply this scheme to a macro-modeled masonry material due to its anisotropic nature.
The transformed-tensor method is based on assuming the existence of a *real anisotropic space* of stresses $\boldsymbol{\sigma}_{ij}$ and a conjugate space of strains $\boldsymbol{\varepsilon}_{ij}$, such that each of these spaces has its respective image in a *fictitious isotropic space* of stresses $\overline{\boldsymbol{\sigma}}_{ij}$ and strains $\overline{\boldsymbol{\varepsilon}}_{ij}$, respectively. The corresponding relationships among them are;

$$\overline{\boldsymbol{\sigma}}_{ij} \overset{\text{def}}{=} A^{\sigma}_{ijkl}\boldsymbol{\sigma}_{kl} \qquad ; \qquad \overline{\boldsymbol{\varepsilon}} \overset{\text{def}}{=} A^{\varepsilon}_{ijkl}\boldsymbol{\varepsilon}_{kl} \tag{8}$$

where A^{σ}_{ijkl} and A^{ε}_{ijkl} are the transformation tensors, for stress and strain, respectively, relating the fictitious and real spaces. These four-rank tensors embody the natural anisotropic properties of the material.
The stress transformation tensor A^{σ}_{ijkl} is a result of the properties of the materials and the shape of the yield surface, namely,

$$A^{\sigma}_{ijkl} = \left(B^{\sigma}_{ijkl}\right)^{-1} = \left(W_{ijrs}\alpha_{rskl}\right)^{-1} \tag{9}$$

where, W_{ijrs} contains information on the yield stress along every axis of orthotropy, and α_{rskl} is the shape adjustment tensor (section 6 ref. (Oller et al. 2003)). The relationship between the stress and strain transformation tensors can therefore be expressed as

$$A^{\varepsilon}_{rsmn} = \left[\overline{C}^{\sigma}_{rsij}\right]^{-1} A^{\sigma}_{ijkl}C^{\sigma}_{klmn} \tag{10}$$

where $\overline{C}^{\sigma}_{rsij}$ and C^{σ}_{klmn} represent the constitutive tensor in the fictitious and real space, respectively.

Steel The most common approach to represent the behavior of ductile materials, such as steel, is via a macro-mechanical theory of plasticity (Kojić and Bathe 2005) based on the notions of a yield surface giving the yield condition, a hardening rule and on the stress-plastic strain relations of the given material.
The concepts of classic plasticity can be extended to plastic damage models, like the one proposed by Oller in (Oller 1998) or Martinez (Martinez et al. 2015), where it is used a normalized internal variable to represent the plastic damage κ^p. Range of values for κ^p are $0 \leq \kappa^p \leq 1$, such that if $\kappa^p = 0$ there is no plastic damage, and $\kappa^p = 1$ defines the total damage of a solid.
There are also other CDM which include the presence of permanent deformations on the mechanical behavior of geomaterials (Jason et al. 2006; Lubliner et al. 1989; Mazars and Pijaudier-Cabot 1989; Tao and Phillips 2005) especially in concrete subjected to compression, where the internal variables are represented by damage variables and also for the permanent plastic deformation.
The idea of using one single damage variable in a general form has been explored by Paredes (Paredes 2013) to be applied in the assessment of the natural frequency of vibration of structures. Paredes considers the different existing possibilities to define the damage index d, and proposes the index d^{eqv} be a function of the yield surface $f(\boldsymbol{\sigma}_0)$ defined as:

$$d^{eqv} = 1 - \frac{f(\boldsymbol{\sigma}_0^c)}{f(\boldsymbol{\sigma}_0)} \tag{11}$$

hence, is now possible to use the damage index d^{eqv} in equation 7 to obtain an equivalent secant tensor. In equation 11 $f(\boldsymbol{\sigma}_0)$ is evaluated with the current tensor of stress, whereas $f(\boldsymbol{\sigma}_0^c)$ is evaluated with the tensor of effective stresses that define the damage threshold of the material which is defined as

$$\boldsymbol{\sigma}_0^c = \begin{bmatrix} f_0^* & 0 & 0 \\ 0 & 0 & 0 \\ 0 & 0 & 0 \end{bmatrix} \tag{12}$$

where f_0^* is nominal threshold of the material's resistance. For the case of concrete, such threshold is defined by the resistance to compression, whereas for ductile materials such as steel, it is defined by the yield stress.
Finally, the use of equation 11 takes to the modification of equation 7 resulting in equation 13.

$$\mathbf{D}^{sec} = (1 - d^{eqv})\mathbf{D}_0 \tag{13}$$

In this work, mechanical behavior of steel will be reproduced using the governing equations of classical rate-independent plasticity model (Simo and Hughes 1998) projected onto the plane-stress subspace and combined with a von Mises yield function.

Mixing theories

In a general sense, a mixing theory is a weighted mean proposed for modeling non-linear mechanical behavior of composite materials made up of continuum or unidirectional fibers.

CMT (**C**lassical **M**ixing **T**heory) was firstly studied by Truesdell and Toupin (Truesdell and Toupin 1960) establishing the basis for subsequent developments, like the ones made by Ortiz and Popov (Ortiz and Popov 1982), Oller *et al* (Oller et al. 1993) and Oñate *et al* (Oñate et al. 1991).

CMT takes into account the volume fraction of components but not its morphological distribution, being this a strong limitation to predict the behavior of most composites.

Modifications to this theory were developed by Rastellini (Rastellini 2006) making the composite behavior dependent on the constitutive laws of component materials according to their volume fractions and to their morphological distribution inside the composite.

The Serial-parallel (SP) mixing theory proposed by Rastellini (Rastellini 2006) assumes that components behave in parallel (iso-strain condition) in the fibers direction and in serial (iso-stress condition) in the orthogonal directions. This work will simulate the composite materials with the SP mixing theory, following the approach used by Martinez in (Martínez 2008).

PROPOSED METHODOLOGY

From a computational-cost point of view, the only viable strategy to perform the analysis of structures built from a large number of masonry units and joints, confined by RC elements with different reinforcement patterns, is using a smeared-cracking and the macro-modeling strategy. Hence the present section focuses on the definition of information related to the composite materials. It also focuses on the meshing requirements in order to carry out the analysis of such structures. An a priori concern in the proposed scheme is that the computational process in terms of time-consuming and RAM (**R**andom **A**ccess **M**emory) needed would be rather expensive. Hence, as an attempt to overcome such disadvantage some alternatives have been explored, and are listed in this section.

Thickness discretization for structural elements

The shell element model used in this work is able of reproducing the out-of-plane degradation due to bending stresses. In order to reproduce this effect with a higher accuracy, becomes mandatory to perform a finer layer distribution of the laminated materials in the following cases (Escudero 2015):

- At the farthest zones away from the geometric axis of the shell, since such layers will be subjected to the higher stresses while acting a bending stress.
- At zones where exist a abrupt change of stiffness, as is the case of the presence of steel reinforcement within the concrete, no matter their position within the overall thickness.

Meshing and composite materials generation

To cover the meshing needs, is selected the use of a pre and post processor for numerical simulations, in this case GiD (CIMNE 2015). GiD is a universal, adaptive and user-friendly pre and post-processor for numerical simulations in science and engineering designed to cover all the common needs in the numerical simulations field from pre to post-processing: geometrical modeling, effective definition of analysis data, meshing, data transfer to analysis software, as well as the visualization of numerical results. The process to obtain the required information to model a large structure formed by laminated materials where each layer are composite materials can be a cumbersome task. This because within the laminated material not only changes the orientation of the fibers, but also the thickness of the layer, and consequently, the volume participation of fiber and matrix. So, in order to overcome this situation, and being able to reproduce *real life* structures in term of steel reinforcement patterns, a computational tool has been developed having in mind the 3 principal requisites shown below.

1. It must be capable of reproducing a more realistic steel reinforcement pattern.
2. It has to be a mechanized process where volume participation of components on a composite materials are generated automatically.
3. It has to be capable of handling information of large meshes.

Such tool arises as a need of mechanizing and generate the composite material information given a large mesh of triangular finite elements and a *real life* steel reinforcement pattern of every layer within the composite. To achieve this, it is necessary to read pre-defined text files, where the information regarding the steel reinforcement patterns has been stored.

The starting point of the generation of the composite materials presented here, is something called *structured composite material* (`SCM` from now on), where a pattern is selected to represent both, the reinforcement steel within layers and the `SCM`'s boundary. Main idea behind the use of this method, is making as mechanical as possible the generation of the composite material for every layer of the FE.

A reader experienced in computer drawing design (using AutoCAD), would find similarities of a `SCM` with a *hatch*. Namely, both are a general pre-generated pattern of bi-dimensional closed polygons (steel reinforcement in the case of a `SCM`) stored in a text file, such pattern is ready to be used as much as needed, and becomes particular, once is given to it, information such as: a contour, a local *x', y'* plane and an insertion point. Then the code on purpose will take care of generate information such as: volume participation, fibers direction (when applicable), and thickness for every layer of the `SCM`. The process to generate such information is carried out as follows:

1. Is generated the text file containing information related to all `SCM` within

the model, also boundaries and insertion points are included.

2. FE mesh is generated for the model (using GiD).
3. The code on purpose searches for the FE's intersecting the contour of the `SCM`.
4. With the FE's intersecting the given `SCM`, volume participation of the matrix ${}^{m}k$ and fiber ${}^{f}k$ for each layer are evaluated using the intersecting area of the steel reinforcement with the FE. In the case, when ${}^{f}k = 0$ the classic mixing theory is selected, whereas serial-parallel mixing theory shall be used if ${}^{f}k \neq 0$.
5. Finally, in order to reduce the number of composite materials, a smoothing for the volume participation of fiber is used.

Let us consider figures 1 as an aid for a better explanation of the proposed method. Figure 1 shows structural drawings of a building with columns type `C-01` and beams type `B-01`, it is also shown the distribution of the steel reinforcement for the concrete slab.

Using the proposed scheme, to model structure on figure 1 a total of three *SCM* will be required. The first one (`SCM-01`), represents the frame of both; axis `1` and `2`, the second one (`SCM-02`) represents only the beams along construction axis `A` and `B`. Finally, a third one (`SCM-03`) will be needed to represent the concrete slab. Section `X-X'` from figure 1 can be seen as `SCM-01`, since it can be repeated over axis `1` and axis `2`. Using figure 2 as a reference, step **1** of the proposed method, is to generate the information of the `SCM`, the starting point is the cross section of the corresponding structural elements (fig. 2.a) to later define the contour, and an insertion point A to refer the reinforcement pattern of all layers to such point (2.d).

Once the mesh has been generated (step **2**) the code on purpose searches for the FE's intersecting the contour of the `SCM`. Figure 2.c depicts the result of step **3** (`SCM-01` at constructive axis `2`). Step **4** consists in overlapping the reinforcement pattern and the intersecting FE's of a given `SCM` to obtain the volume participation of the matrix ${}^{m}k$ and fiber ${}^{f}k$, and the fiber direction for each layer (fig. 2.d). Finally, step **5** is performed to reduce the amount of composite materials generated.

Computational strategy

In this section are described the improvements performed in PLCd (CIMNE 2014), in order to make possible to analyze large structures in a reasonably short amount of time. PLCd (CIMNE 2014) is a state of the art implicit finite element code written in Fortran, and originally developed by Prof. Oller at CIMNE. It has been developed to treat a large variety of composite materials through the use of Rules of Mixtures.

Time-based optimization

The optimization process in terms of time has been carried out using a parallelization scheme with OpenMP (Barney et al. 2010) directives in three different

sections of the code. Such sections are shown below.

1. Loop over elements while evaluating the generalized strains $\hat{\boldsymbol{\varepsilon}}$ and the generalized stresses $\hat{\boldsymbol{\sigma}}$.
2. Loop over elements while integrating the constitutive equations (plasticity, damage, etc.). In this portion of the code the goal is to evaluate internal forces of each FE so they can be assembled into a global vector usually referred to as $\mathbf{LHS}_g$. Hence, the elemental $\mathbf{LHS}_e$ can be evaluated in different threads to later be assembled restricting the access to the $\mathbf{LHS}_g$ vector to only one thread at the time.
3. Loop over elements while writing/reading information to perform a restart operation.

Memory-consuming optimization

A scheme using user-defined data types was implemented, where, at the beginning of the analysis process, the information is reserved and only allocated while needed (once the FE is in a non-linear range), leading to a less necessity of RAM memory resources. Starting from the assumption that not all elements reach a non-linear behavior, the proposed programming scheme (shown below) was implemented in PLCd.

- It was used a *template* to store internal variable for every non-damaged FE with the same composite information. At this point it is not necessary to store strain or stress information of composite neither components of the laminated material.
- Once a component within a FE has reach a non-linear behavior, then allocation of memory to store information of the FE was required (internal variables, stresses and strains).
- Allocating at every loading step or iteration may be time consuming, however, it will be justified for large structures where a considerable amount of RAM would be required.
- For output and visualization purposes (writing information in GiD format) the information of non-damaged finite elements is evaluated using their local displacements, which can be seen as the major drawback.

Basically, the process followed is this: if any of the components within any layer of the laminated material reach a non-linear range, such FE is considered as damaged, thus, information of the components has to be stored. Otherwise, strains and stresses are evaluated using the local displacements of the finite element.
The use of an iterative solver has also been considered, so, it has been implemented in PLCd the library developed by Vargas and Botello-Rionda (Vargas-Félix and Botello-Rionda 2012), which contains routines running in parallel, to handle and solve the typical linear systems of equations resulting from finite element or finite volume discretizations for a large number of unknowns. In the studied cases only comparisons in terms of consumed memory were carried out,

however, further comparisons in terms of running time while using an iterative solver are required, to fit the best alternative.

NUMERICAL EXAMPLES

In this section two practical examples are proposed and intended to test the capabilities of the proposed analysis scheme. The first one corresponds to an experimental test carried out by Meli (Meli 1979) used in order to reproduce, from an experimental point of view, the isolated behavior of a masonry wall confined with two columns and a beam made of reinforced concrete. The second model corresponds to a construction outlined through structural drawings, sized and structured following the building code regulations for masonry structures in Mexico City. The results obtained using the building code regulation for this structure are for comparative purposes.

Reinforced Concrete Frame With Masonry In-fill

The example reproduced in this section, corresponds to an experimental test carried out by Meli, and fully described in (Meli 1979). Geometry of analyzed specimen is depicted in figure 3, where it is presented a lateral view (fig. 3.a) and a frontal view (fig. 3.b), also it is presented the location of the confining structural elements (`C-01` and `B-01`), the distribution of the masonry units, and the boundary conditions such as, an imposed displacement at the top, and a fixed support at the bottom. Figure 3.b also depicts an overlapping of the crack patterns of the experimental test (Meli 1979). In the present study the masonry in-fill exhibits the typical response that takes place for low resistance masonry units, i.e. crack will cross indistinctly throughout masonry unit or mortar.
To reproduce numerically the present model, three simple materials are involved, mechanical properties of each one of them are described next.

Steel

- Elasticity modulus: $E = 2.1x10^5 MPa$
- Poissons's Ratio: $\upsilon = 0.00$
- Self-weight: $\gamma = 7845 kg/m^3$
- Yield criterion: Von Mises.
- Damage thresholds:

$$\sigma_c = 270 MPa \qquad \sigma_t = 270 MPa$$

- Fracture energy:

$$G_c = 2.0 MPa \cdot m. \qquad G_t = 2.0 MPa \cdot m$$

Concrete Mechanical properties of concrete have been evaluated considering a compression resistance equal to $f'_{cy} = 250 kg/cm^2$ ($24.53x10^6 N/m^2$), to later, evaluate the elasticity modulus according to section `1.5.1.4` of reference (NTC 2004b), namely:

$$E = 4400\sqrt{f'_{cy}} \tag{14}$$

where units of equation 14 are given in MPa. All other mechanical properties needed are shown below.

- Elasticity modulus: $E = 2.18x10^4 MPa$
- Poissons's Ratio: $\upsilon = 0.00$
- Self-weight: $\gamma = 2500kg/m^3$
- Yield criterion: Mohr Coulomb.
- Damage thresholds:

$$\sigma_c = 24.53MPa \qquad \sigma_t = 2.45MPa$$

- Fracture energy:

$$G_c = 50.0KPa \cdot m. \qquad G_t = 5.0KPa \cdot m$$

Masonry Mechanical properties used to reproduce behavior of the masonry in-fill, have been obtained assuming a compression resistance of $f'_m = 40kg/cm^2$ $(3.92MPa)$ and $\upsilon^*_m = 1.1kg/cm^2$ $(0.15MPa)$. Hence, elasticity modulus $E_{mx} = 1.37x10^3 MPa$ according to section `2.8.5.2` of reference (NTC 2004c), where

$$E_{mx} = 350f'_{mcy} \tag{15}$$

elasticity modulus is evaluated under sustained loads (eq. `2.6`) reference (NTC 2004c).

- Elasticity modulus:

$$Emx = 1.37x10^3 MPa$$
$$Emy = 0.73x10^3 MPa$$

- Poisson's ratio: $\upsilon_{xy} = 0.10$, $\upsilon_{yx} = 0.15$
- self-weight $\gamma = 1300kg/m^3$
- Yield criterion: Mohr Coulomb.
- Damage thresholds:

$$\sigma_{mcx} = 3.920MPa \qquad \sigma_{mtx} = 200KPa$$
$$\sigma_{mcy} = 1.270MPa \qquad \sigma_{mty} = 65KPa$$

- Fracture energy:

$$G_c = 20.0KPa \cdot m.$$
$$G_t = 0.2KPa \cdot m$$

Cross section of confining elements are presented in figure 4.a. Both section `C-01` and `B-01` have been discretized using 10 layers with different thickness, since they

have been adjusted to the location of the steel reinforcement. General location of the steel reinforcement is displayed in figure 4.b, there, it can be seen that layers 01, 05, 06 and 10 do not have steel reinforcement, whereas, layer 03 and 08 contain both beam's stirrup steel reinforcement ($\phi 6.4mm$) and column's main steel reinforcement ($\phi 15.9mm$). On the other hand, layers 04 and 07 contain only the main steel reinforcement of beams, and finally, layers 02 and 09 contain only the stirrup steel reinforcement of columns. The analysis has been performed using two lading stages, the first one corresponds to gravity loads evaluated using the self-weight of the corresponding material, the second loading stage correspond to a pushover analysis intended to predict the force-displacement response of the structure.

Comparison among force-displacement response of both, Meli (Meli 1979) and the present work is presented in figure 5.a. Figure 5 from b to d depict the damage state of three different loading steps $\delta_1 = 0.46mm$, $\delta_2 = 1.94mm$ and $\delta_3 = 7.66mm$. Column on the left shows the damage state of layer 01 of the confining elements, column on the center displays the damage state of the masonry in-fill, and finally column on the right shows the stresses in local direction of steel fibers within layer 03.

In both cases depicted in figure 5.a, the response is characterized by a high-stiffness zone at the beginning of the loading process. However, such response is followed by a slight decreasing of stiffness due the separation of the masonry corners and the confining elements, as reported by Meli, such behavior was not captured in the present work leading to a significant difference in the force-displacement response, since only one diagonal crack is starting to grow while performing the numerical simulation, as can be seen in figure 5.b.

Finally, beyond the point where occurs a slight loss of stiffness (δ_2), characterized by the apparition of several diagonal cracks, a better concordance in the response between both testes is observed.

One storey construction

This example is a one-storey construction with the typical dimensions of a bedroom and will serve to highlight the capabilities of the analysis scheme proposed in this work, for now on, such model will be referred to as `B-OSC`.

Building `B-OSC` is structured with load-bearing walls and a roofing system based on a solid reinforced concrete slab. It has a window in the rear façade, and a window and a door in the front façade. Load-bearing walls have been structured to meet the requirements of the masonry code regulation (NTC 2004c) in force for the Mexico City, namely:

- Masonry units meet the minimum width necessary to prevent buckling problems in slender walls, according to section `5.1.4` of reference (NTC 2004c).
- Reinforced concrete elements whose purpose is confining the load-bearing masonry wall, meet the maximum separation among themselves in plan, in addition, also meet the rates of reinforcing steel necessary due bending

and temperature, according to provisions stated in section `5.1.1`, reference (NTC 2004c).

- Openings like doors and windows in masonry load-bearing walls have been reinforced in the whole perimeter using beams and columns, according to provision stated in section `5.1.3`, reference (NTC 2004c).
- The thickness of the roof slab meets the requirements necessary to maintain the deflections within the serviceability limits stated in section `3` of reference (NTC 2004b).

Structural Drawings

The structural drawings for the construction `B-OSC` are shown in figure 6. Effort has been put to make them as close to *real life* construction as possible, especially regarding the distribution of steel reinforcement, where the simplifications that a structural engineer would make for an easy placement in the field. Typically, in all drawings the diameters of the reinforcing steel rods are shown in millimeters, although they correspond to the British nomenclature, where diameters of 6.4mm, 9.5mm y 1.27mm correspond to 1/4", 3/8" y 1/2" respectively, this will be maintained as a common practice in structural drawings presented along this section.

Structural elements

A brief description of the reinforced concrete structural elements involved in the structure of this section is carried out next.

Masonry in-fills Regarding the masonry in-fills, it will only be mentioned that has been discretized using an arrangement of 12 layers whose thickness have been detailed in figure 7.

Columns It has only been selected one cross section for columns, which is shown in figure 8.a, named `Kc-01` and endowed with a main steel reinforcement of 4 rods $\phi 12.7mm$ (1/2"), whereas the secondary steel reinforcement is formed by steel rods $\phi 6.4mm$ (1/4") with a separation among themselves of 15 centimeters. Cross section `Kc-01` has been discretized using an arrangement of 18 layers whose thickness is presented also in figure 8.b.

Beams Two different sections of beams have been selected. The first one named `Kb-01` to be used in the *regular* walls (union of the beam with the concrete slab), and the second one named `Kb-02` to be used in the *lower* walls (walls forming the window opening).
Figure 8.a shows the steel reinforcement pattern and layer distribution of both sections `Kb-01` and section `Kb-02`. The basic difference among them is their height, since in both cases, the main steel reinforcement (4 rods $\phi 12.7mm$) and the secondary steel reinforcement (rods $\phi 6.4mm$ separated 15 centimeters) are

the same. Also, in both cases, the thickness has been discretized using an arrangement of 18 layers (table 8.b).
In both cases, beam sections have a coating for the transverse steel of 33 millimeters (left and right side) and 20 millimeters at the upper and lower part, this is usually done in the field as an adjustment to prevent longitudinal steel overlaps.

Slabs Although simple materials that make up the concrete slab were fixed to have a linear behavior, it has been discretized using a pattern of 20 layers for a total thickness of 15 centimeters (9.b). Layer distribution of reinforced concrete slab can be seen in figure 9.a, where also can be noticed the steel reinforcement in both beds and in both orthogonal directions. The diameter of the steel reinforcement rods are $\phi 9.5mm$ (3/8"), also can be noticed the different separation among themselves, which for the lower bed is 30 centimeters, whereas for the upper bed is 40 centimeters.

Simple material properties

Only three simple materials are needed to perform the analysis of models presented in this section, namely: steel, concrete and masonry. Their mechanical and constitutive properties are detailed next.

Steel

- Elasticity modulus: $E = 2.1x10^5 MPa$
- Poissons's Ratio: $\upsilon = 0.00$
- Self-weight: $\gamma = 7845kg/m^3$
- Yield criterion: Von Mises.
- Damage thresholds:

$$\sigma_c = 420MPa \qquad \sigma_t = 420MPa$$

- Fracture energy:

$$G_c = 2.0MPa \cdot m. \qquad G_t = 2.0MPa \cdot m$$

Concrete The compressive strength is assumed equal to $f'_c = 250kg/cm^2$ ($24.53x10^6 N/m^2$). The elasticity modulus is evaluated according section `1.5.1.4` of reference (NTC 2004c), namely:

$$E = 4400\sqrt{f'_{cy}} \tag{16}$$

where units of equation 16 are given in MPa. All other mechanical properties needed are shown below.

- Elasticity modulus: $E = 2.5x10^4 MPa$
- Poissons's Ratio: $\upsilon = 0.20$

- Self-weight: $\gamma = 2500kg/m^3$
- Yield criterion: Mohr Coulomb.
- Damage thresholds:

$$\sigma_c = 25.0MPa \qquad \sigma_t = 3.50MPa$$

- Fracture energy:

$$G_c = 50.0KPa \cdot m. \qquad G_t = 5.0KPa \cdot m$$

Masonry The mechanical properties of masonry described in this section, have been obtained assuming that simple compressive strength (f_{mcy}) of the combination of masonry units and mortar is equal to $f_m^* = 120kg/cm^2$, whereas the maximum shear strength is equal to $\upsilon_m^* = 3.5kg/cm^2$. Once such parameters have been settled, using 17 ((NTC 2004c)) is now possible to define the elasticity and shear modulus. Other mechanical and constitutive properties are described below.

$$\begin{aligned} E_m = E_1 = E_2 = 600 f_m^* = 7.06x10^3 MPa \\ G_{xy} = 0.4 E_m = 2.825x10^3 MPa \end{aligned} \tag{17}$$

- self-weight $\gamma = 1500kg/m^3$
- Yield criterion: Mohr Coulomb.
- Damage thresholds:

$$\begin{aligned} f_{mcx} = 5.15MPa \qquad & f_{mtx} = 350KPa \\ f_{mcy} = 12.00MPa \qquad & f_{mty} = 600KPa \end{aligned}$$

- Fracture energy:

$$\begin{aligned} G_c = 20.0KPa \cdot m. \\ G_t = 0.5KPa \cdot m \end{aligned}$$

Composite material generation

Since the used methodology to obtain the volume fraction for the composite materials belonging to a laminated shell has already been described in section 3 of this work, in this section is only mentioned the case of a `SCM`, corresponding to the concrete slab (figure 10). Only finite elements belonging to the given `SCM` have been plot, also has been plot the contour of the slab, the steel reinforcement, and the contour of the remaining `SCM` for reference purposes. In both cases only is shown the bottom steel reinforcement.

In figures on the right are depicted the corresponding FE with ${}^f k > 0$.

Boundary conditions

Analysis process has been performed using 3 different loading phases. It is convenient to point out that in none of the 3 loading phases have been used the

loading factors that are normally included in building code regulations, neither have been used security factor for designing purposes. Analysis has been performed in this way on purpose, so results obtained using a design code can be properly compared with the results obtained using the scheme proposed in this work.

Fixed displacements In all loading phases, the basement of the structure has been set to remain rigidly fixed, hence, neither displacements nor rotations will be allowed.

First stage loading condition: Dead loading This loading condition corresponds to combined weight of the elements with structural purpose plus the weight of the elements belonging to the structure without a structural purpose and only used to fulfill architectural requirements. A small sketch (fig. 11 left) of structural and architectural elements belonging to masonry walls is displayed. It is also shown a table displaying thickness and weight of all components involved.

Figure 11 on the right also shows a dead loading analysis; in this case, it is about the roofing system. As in the previous example, on the left is shown a sketch pointing all materials involved, while in the right part a table detailing weights and thicknesses are displayed. Also due the recommendation of article `197` of reference (RCD 1993), it will be added $40kg/m^2$, yielding to the total weight due to the presence of concrete and mortar $D_L \approx 525.0kg/m^2$.

Second stage loading condition: Live loading Live loads, are temporary and of short duration (while compared to permanent loads), such loads are based upon published regulations, in the case of this work, it has been used the *Reglamento de construcciones para el Distrito Federal* (RCD 1993) to predict them. Such code regulation in its chapter V article `199.V.g`, marks a uniform load of 100 kg/m^2 to be used in the roof for residential homes, being only valid when the slope of the roof is less or equal to 5%.

Third stage loading condition: Pushover Finally, the third loading stage corresponds to a pushover applied separately in both orthogonal direction x and y. Hence, for both directions the displacements displayed in figure 12 have been imposed and their purpose is to predict the force-displacement response of the structure. Obtained results are detailed next.

Reference solution - Building code

Figure 13 (on the left) shows a numeration for masonry walls and their total length, it is important to state a numeration like this, since most of the results presented next will be referred to it. On the right side of the same figure, the tributary load of each masonry wall is presented. The total amount of bear-loading masonry walls is 5.

For the analysis purposes regarding the code regulation (NTC 2004c), the *short* walls that form part of the window have not been considered, nor the stiffness due to reinforced concrete confining elements.

It is also necessary to point out that according to the *detailed* analysis shown in reference (NTC 2004c), the walls perpendicular (in plan view) to the analysis direction have to be neglected, hence, in such cases, stiffness and shear strength is equal to 0. Thus, to evaluate the total stiffness and shear strength of the structure in X direction, only have to be considered walls `W-01` and `W-02` (fig. 13), while for direction Y only walls `W-03`, `W-04` and `W-05` have been considered.

Table 1 displays the stiffness and shear strength of the masonry walls evaluated according to reference (NTC 2004c). From table 1 can be inferred the total stiffness of the structure in both orthogonal directions presented in 18.

$$\mathbf{K}_x = 948005.44kN/m \quad ; \quad \mathbf{K}_y = 56602.81kN/m \tag{18}$$

also from table 1 it is possible to obtain the total shear strength of the structure in both orthogonal direction, this is:

$$\mathbf{V}_R^x = 443.12kN \quad ; \quad \mathbf{V}_R^y = 168.07kN \tag{19}$$

values shown in 18 and 19 will be used as a comparison point.

Result comparison X-direction analysis

The response of the structure when the displacement has been applied in X direction will be described using the graph of figure 14. There, the combined response of walls `W-03, W-04` and `W-05` will be referred as *shell-acting* walls, or simply *shell* walls, since their ability to restrict displacements in X direction is given by their flexural stiffness. On the other hand, the combined response of walls `W-01` and `W-02` is referred as *membrane-acting* walls or simply *membrane* walls, since their ability to avoid displacements in X direction is given by their membrane stiffness acting as cantilever beams whose height is equal to the corresponding length of the masonry wall. Finally, in red is shown the combined response of both *membrane* and *shell* walls.

In graph from figure 14 can be noticed the well agreement among the stiffness evaluated using reference (NTC 2004c) and total stiffness of masonry walls evaluated with the proposed scheme even though neither concrete or steel stiffness are considered by reference (NTC 2004c). Not only stiffness shows a reasonably good agreement, also the total shear strength does, which in the case of reference (NTC 2004c) is defined as the point where non-linear process would begin. The graph shown in figure 14 also confirms reference (NTC 2004c) regarding the low stiffness presented by *bending* walls and that they can be neglected for analysis and design purposes. In order to carry out a proper description of the displacement-force response graph, it has been divided into 6 segments, this is:

- Segment $\overline{\mathbf{OA}}$, where the elastic response occurs.

- Segment $\overline{\mathbf{AB}}$, where the first crack appears, reaching the maximum shear strength of the entire structure in x direction at point **B**.
- Segment $\overline{\mathbf{BC}}$ corresponds to the process of spending the entire capability of masonry walls to support lateral forces, beyond **C** point, high discontinuities are expected, since the resistance due lateral forces are only provided by the confining elements.
- Segment $\overline{\mathbf{CD}}$ is a sudden lost of stiffness due the rupture of confining elements at one of the points where the loads have been applied.
- Segment $\overline{\mathbf{DE}}$ can be described as a small amount of lateral force that the structure is able to support until the next rupture of a confining element occurs.
- And finally, segment $\overline{\overline{\mathbf{EF}}}$ which is the sudden rupture of other confining element at the point where the displacement is imposed.

Figure 15 is a set of images displaying the undergoing deformation from a frontal perspective where mostly can be appreciated the principal façade and the masonry wall `W-01`, although is also visible the wall `W-02`. In all cases the deformation has been amplified 200 times, image of case a correspond to the undeformed mesh. Figures b, c and d display the crack patterns of the masonry in-fill for three different loading steps, whereas figures e and f display the damage undergone in the confining RC elements.

Result comparison Y-direction analysis

From the performed analysis in Y direction, the first inference obtained is the low stiffness of the structure while compared with the X direction. Let us consider the displacement-force graph of figure 16, where the same consideration regarding *bending* and *masonry* walls have been made as in the X direction analysis. In this case, the *bending-acting* walls are `W-01` and `W-02`, whereas `W-03`, `W-04` and `W-05` are the *membrane-acting* walls. In figure 16 are represented the contribution of the walls separately, the overall response, the total stiffness and the total shear strength obtained according to reference (NTC 2004c).

The first observation from the displacement-force response, is the evident mismatch among stiffness evaluated using reference (NTC 2004c) and the results obtained using the proposed scheme. Apart from the omission of steel and concrete, such mismatch is because of the contribution of *short* walls (walls forming the windows openings), since they act as stiffeners shortening the total height of the adjacent walls. To better point out the stiffener effect of short walls let us consider table **??**, where is reported the stiffness evaluated of the *shortened* walls, this is, reducing their total height in such a way it is not considered from the top of the *short* walls to the basement. If we make such consideration, the reported stiffness is $\mathbf{K}_y = 219404.31 kN/m$ (table **??**), which lead to a more precise prediction of the total stiffness.

As in the previous section, the displacement-force graph (fig. 16) also has been divided into segments in order to carry out a proper description, such segments are described in next paragraph.

- Segment $\overline{\mathbf{OA}}$, is where the elastic response occurs, reporting a total stiffness $\mathbf{K} = 291981.95kN/m$ which is 5.15 times the stiffness evaluated using reference (NTC 2004c). At the light of this result, it can be said that short walls should be included to obtain a more accurate evaluation of the stiffness.
- Segment $\overline{\mathbf{AB}}$, corresponds to the propagation of the cracks, reaching the maximum shear strength of the structure at point **B**. It can be appreciated a well agreement among both shear strengths, the one evaluated using reference (NTC 2004c) with the maximum shear strength obtained using the proposed scheme.
- And finally, segment $\overline{\mathbf{BC}}$ where the resistance of the structure start to decrease, until it reaches point **C**, beyond such point, appears a sudden loss of stiffness due to the rupture at the bottom corner of the confining elements in the walls of the rear façade.

As in previous section, a set of images (figure 17) is used to describe the damage evolution, and all cases the deformation has been amplified 500 times, except for the case *a* that corresponds to the reference mesh. Figure 17.b displays a point (at a imposed displacement equal to $0.4726mm$) where the non-linear process starts, as can be seen, a timid damage process starts in wall `W-03` in the union of confining column `Kc-01` with the brickwork. Next, the crack propagates vertically along wall `W-03` (figures 17.c and 17.d) until it reaches the horizontal confining element at the top (beam `Kb-01`), then the crack propagates diagonally until it reaches the confining element `Kb-02`. Also in figures 17.e and 17.f can be appreciated a slight damage of the confining element at the corners of the window openings. It is necessary to point out that the damage process at the bottom (from the bottom of the window opening to the foundation of the wall) of wall `W-03` is almost zero due to the small tensional stress which the wall is subjected to in such area, same happens in wall `W-04` and `W-05`.

CONCLUSIONS

This work deals with the analysis of large masonry structures, where a methodology to analyze them has been developed, implemented in the context of the finite element method, and finally, compared with building regulations obtaining good results.

The starting point of this work has been the use of a 3-node and 2-dimensional triangular shell element with one Gauss point combined with the state-of-the-art rule of mixtures theories for composite materials (Escudero 2015). Thus, make it possible to use composite materials whose components can be modeled with non-linear constitutive equations. Although the proposed methodology has only been applied to masonry structures in the present study, it can easily be extended to frame structures with or without masonry in-fills. Other conclusions regarding the development of this work are listed below.

- The use of a macro-modeling technique combined with *plain* finite elements

has proven been effective, and it is possible to obtain good concordance among modeled structures and the results obtained using references (RCD 1993; NTC 2004a; NTC 2004b; NTC 2004c; NTC 2004d).

- It has been proved the significant difference among the stiffness of masonry walls when their planes are perpendicular (*bending-acting* walls) or parallel (*membrane-acting* walls) to the direction of the acting force. Such effect has been taken into account for most of the construction code regulations, assuming the higher damage will occur on the *membrane-acting* walls, and despising for designing purposes, the *bending-acting* walls, which coincides with obtained results of this work.
- In the studied cases of this work, has been observed the stiffener effect produced by the *short* masonry walls formed at the windows openings that entirely change the stiffness, and consequently, the structural behavior of the adjacent masonry walls.

In order to be able to reproduce the steel reinforcement pattern of *real-life* constructions, a computational tool was developed having in mind the 3 principal requisites shown next:

1. It should reproduce a more realistic reinforcement pattern.
2. It should mechanize a process where volume part of components within a composite material is generated.
3. It should be capable of handling information of large meshes.

Finally, it has to be stated that due to the size of the models considered in this work, it is necessary to adopt a programming strategy that allow to reduce the execution time of analysis, and also to reduce the computational resources required in terms of memory RAM. The strategies described in this document have proved valid, as they have allowed to obtain the presented results with a reasonable computational cost.

ACKNOWLEDGEMENTS

This work has been supported by the European Commission, under the Marie Curie program, at the IRSES agreement `612607` (TCAINMAND project), by the European Research Council through of the Advanced Grant: `ERC-2012-AdG 320815 COMP-DES-MAT` *Advanced tools for computational design of engineering materials*, by the European Community under grant: `NMP-2009-2.5-1 246067` *Multiscale Reinforcement of Semi-crystalline Thermoplastic Sheets and Honeycombs*, and by the the Mexican government through the grant provided by CONACyT to complete the PhD studies. All this support is gratefully acknowledged.

REFERENCES

Reglamento de Construcciones del Distrito Federal. (1993). México, D.F.

Normas Técnicas Complementarias para Diseño por Sismo (2004a). México, D.F.

Normas Técnicas Complementarias para Diseño y Construcciones de Estructuras de Concreto (2004b). México, D.F.

Normas Técnicas Complementarias para Diseño y Construcciones de Estructuras de Mampostería (2004c). México, D.F.

Normas Técnicas Complementarias sobre Criterios y Acciones para el Diseño Estructural de las Edificaciones (2004d). México, D.F.

Allman, D. (1984). "A compatible triangular element including vertex rotations for plane elasticity analyses." *Computer & Structures*, 19(1-2), 1–8.

Barney, B. et al. (2010). "Introduction to parallel computing." *Lawrence Livermore National Laboratory*, 6(13), 10 https://computing.llnl.gov/tutorials/openMP/#Introduction.

Batoz, J.-L. (1982). "An explicit formulation for an efficient triangular plate-bending element." *International Journal for Numerical Methods in Engineering*, 18(7), 1077–1089.

Batoz, J.-L., Bathe, K.-J., and Ho, L.-W. (1980). "A study of three-node triangular plate bending elements." *International Journal for Numerical Methods in Engineering*, 15, 1771–1812.

Bazant, Z. P. and Pijaudier-Cabot, G. (1989). "Measurement of characteristic length of nonlocal continuum." *Journal of Engineering Mechanics*, 115(4), 755–767.

Bergan, P. and Felippa, C. (1985). "A triangular membrane element with rotational degree of freedom." *Computer Methods in Applied Mechanics and Engineering*, 50, 25–69.

Brzev, S. (2007). *Earthquake-resistant confined masonry construction*. NICEE, National Information Center of Earthquake Engineering, Indian Institute of Technology Kanpur.

Chaboche, J. (1988a). "Continuum damage mechanics: Part i-general concepts." *Journal of Applied Mechanics*, 55(1), 59–64.

Chaboche, J. (1988b). "Continuum damage mechanics: Part ii—damage growth, crack initiation, and crack growth." *Journal of Applied Mechanics*, 55(1), 65–72.

CIMNE (1991-2014). *PLCd - Non-linear thermomechanic finite element code (http://www.cimne.com/PLCd)*. International Center of Numerical Methods in Engineering, Barcelona, España. Finite element code oriented to PhD student education.

CIMNE (2015). *GiD - Adaptive and user-friendly pre and postprocessor for numerical simulations in science and engineering*. International Center of Numerical Methods in Engineering, Barcelona, España. http://www.gidhome.com/.

Eijo, A. (2014). "Finite element modelling of delamination in advanced composite beams and plates using one- and two-dimensional finite elements based on the refined zigzag theory.." PhD dissertation, Escola Tècnica Superior D'Enginyers de Camins, Canals I Ports. Universitat Politècnica de Catalunya, Barcelona, España.

Escudero, C. (2015). "Numerical calculation model for the global analysis of con-

crete structures with masonry walls." Ph.D. thesis, Escola Tècnica Superior D'Enginyers de Camins, Canals I Ports. Universitat Politècnica de Catalunya, Barcelona, España.

Escudero, C., Oller, S., Martinez, X., and Barbat, A. H. (2016). "A laminated structural finite element for the behavior of large non-linear reinforced concrete structures." *Finite Elements in Analysis and Design*, 119, 78–94.

Esteva, L. (1961). "Comportamiento de muros de mampostería sujetos a carga vertical." *Instituto de Ingenieria, Universidad Nacional Autonoma de Mexico*.

Esteva, L. (1963). "Estimaciones de daños probables producidos por temblores en edificios." *Instituto de Ingenieria, Universidad Nacional Autonoma de Mexico*.

Esteva, L. (1966). "Behaviour under alternating loads of masonry diaphragms framed by reinforced concrete members." *Proceedings of the International Symposium on the Effects of Repeated Loadings of Materials and Structures*, V, 1–36.

Faria, R., Oliver, J., and Cervera, M. (1998). "A strain-based plastic viscous-damage model for massive concrete structures." *International Journal of Solids and Structures*, 35(14), 1533–1558.

Felippa, C. (2003). "A study of optimal membrane triangles with drilling freedom." *Computer Methods in Applied Mechanics and Engineering*, 192(16), 2125–2168.

Fundación, I. (1999). *Edificaciones de mampostería para vivienda*. Fundación ICA.

Hernández, O. (1975). "Recomendaciones para el diseño y construcción de estructuras de mampostería." *Instituto de Ingeniería, Universidad Nacional Autónoma de México*.

Hillerborg, A., Modéer, M., and Petersson, P.-E. (1976). "Analysis of crack formation and crack growth in concrete by means of fracture mechanics and finite elements." *Cement and concrete research*, 6(6), 773–781.

Hughes, T. and Brezzi, F. (1989). "On drilling degrees of freedom." *Computer Methods in Applied Mechanics and Engineering*, 72, 105–121.

Jason, L., Huerta, A., Pijaudier-Cabot, G., and Ghavamian, S. (2006). "An elastic plastic damage formulation for concrete: Application to elementary tests and comparison with an isotropic damage model." *Computer methods in applied mechanics and engineering*, 195(52), 7077–7092.

Ju, J. (1989). "On energy-based coupled elastoplastic damage theories: constitutive modeling and computational aspects." *International Journal of Solids and Structures*, 25(7), 803–833.

Khosravi, P., Ganesan, R., and Sedaghati, R. (2007). "Corotational non-linear analysis of thin plates and shells using a new shell element." *International Journal for Numerical Methods in Engineering*, 69, 859–885.

Kojić, M. and Bathe, K.-J. (2005). *Inelastic analysis of solids and structures*. Springer.

Lemaitre, J. (1985). "Coupled elasto-plasticity and damage constitutive equations." *Computer Methods in Applied Mechanics and Engineering*, 51(1), 31–

974 49.
975 Lourenço, P. (1996). "Computational strategies for masonry structures." PhD
976 dissertation, Delft University, Delft, Netherlands.
977 Lourenco, P. B., Milani, G., Tralli, A., and Zucchini, A. (2007). "Analysis of ma-
978 sonry structures: review of and recent trends in homogenization techniques.."
979 *Canadian Journal of Civil Engineering*, 34(11), 1443–1457.
980 Lubliner, J., Oliver, J., Oller, S., and Oñate, E. (1989). "A plastic-damage model
981 for concrete." *International Journal of Solids and Structures*, 25(3), 299–326.
982 Madinaveitia, M. (1971). "Ensayes de muros de mampostería con cargas
983 excéntricas." *Instituto de Ingenieria, Universidad Nacional Autonoma de Mex-*
984 *ico*.
985 Madinaveitia, M. and Rodríguez, G. (1970). "Resistencia a carga vertical de
986 muros fabricados con materiales usuales en el distrito federal." *Instituto de*
987 *Ingenieria, Universidad Nacional Autonoma de Mexico*.
988 Martínez, X. (2008). "Micro-mechanical simulation of composite materials us-
989 ing the serial/parallel mixing theory." Ph.D. thesis, Escola Tècnica Superior
990 D'Enginyers de Camins, Canals I Ports. Universitat Politècnica de Catalunya,
991 Barcelona, España.
992 Martinez, X., Oller, S., Barbu, L. G., Barbat, A., and De Jesus, A. (2015).
993 "Analysis of ultra low cycle fatigue problems with the barcelona plastic damage
994 model and a new isotropic hardening law." *International Journal of Fatigue*,
995 73, 132–142.
996 Mazars, J. and Pijaudier-Cabot, G. (1989). "Continuum damage theory-
997 application to concrete." *Journal of Engineering Mechanics*, 115(2), 345–365.
998 Meli, R. (1979). *Comportamiento sísmico de muros de mampostería*. Instituto de
999 Ingenieria, Universidad Nacional Autonoma de México, México, D.F., second
1000 edition (May).
1001 Meli, R. and Alcocer, S. M. (2004). "Implementation of structural earthquake-
1002 disaster mitigation programs in developing countries." *Natural Hazards Review*,
1003 5(1), 29–39.
1004 Meli, R. and Hernández, O. (1971). "Propiedades de piezas para mampostería
1005 producidas en el distrito federal." *Instituto de Ingeniería, Universidad Nacional*
1006 *Autonoma de México*.
1007 Meli, R. and Hernández, O. (1975). "Efectos de hundimientos diferenciales en
1008 construcciones a base de muros de mampostería." *Instituto de Ingenieria, Uni-*
1009 *versidad Nacional Autonoma de Mexico*.
1010 Meli, R. and Reyes, A. (1971). "Propiedades mecánicas de la mampostería."
1011 *Instituto de Ingenieria, Universidad Nacional Autonoma de Mexico*.
1012 Meli, R. and Salgado, G. (1969). "Comportamiento de muros de mampostería su-
1013 jetos a carga lateral." *Instituto de Ingenieria, Universidad Nacional Autonoma*
1014 *de Mexico*.
1015 Meli, R., Zeevart, W., and Esteva, L. (1968). "Comportamiento de muros de
1016 mampostería hueca ante carga lateral alternada." *Instituto de Ingenieria, Uni-*
1017 *versidad Nacional Autonoma de Mexico*.

Oliver, J., Cervera, M., Oller, S., and Lubliner, J. (1990). "Isotropic damage models and smeared crack analysis of concrete." *Second international conference on computer aided analysis and design of concrete structures*, Vol. 2, 945–958.

Oller, S. (1998). "Un modelo de daño continuo para materiales friccionales." Ph.D. thesis, Escola Tècnica Superior D'Enginyers de Camins, Canals I Ports. Universitat Politècnica de Catalunya, Barcelona, España.

Oller, S., Car, E., and Lubliner, J. (2003). "Definition of a general implicit orthotropic yield criterion." *Computer methods in applied mechanics and engineering*, 192(7), 895–912.

Oller, S., Oñate, E., Miquel Canet, J., and Botello, S. (1993). "A finite element model for analysis of multiphase composite materials." *ICCM/9.*, Vol. 3, 94–103.

Oñate, E., Oller, S., Botello, S., and Canet, J. M. (1991). *Métodos avanzados de cálculo de estructuras de materiales compuestos*. Centro Internacional de Métodos Numéricos en Ingeniería (CIMNE).

Ortiz, M. and Popov, E. P. (1982). "Plain concrete as a composite material." *Mechanics of Materials*, 1(2), 139–150.

Paredes, J. A. (2013). "Modelización numérica del comportamiento constitutivo del daño local y global y su correlación con la evolución de las frecuencias naturales en estructuras de hormigón reforzado." PhD dissertation, Escola Tècnica Superior D'Enginyers de Camins, Canals I Ports. Universitat Politècnica de Catalunya, Barcelona, España.

Paredes, J. A., Barbat, A. H., and Oller, S. (2011). "A compression–tension concrete damage model, applied to a wind turbine reinforced concrete tower." *Engineering Structures*, 33(12), 3559–3569.

Pelà, L. (2009). "Continuum damage model for nonlinear analysis of masonry structures." Ph.D. thesis, Università degli studi di Ferrara, Ferrara, Italy.

Rastellini, F. G. (2006). "Modelación numérica de la no-linealidad constitutiva de laminados compuestos." Ph.D. thesis, Escola Tècnica Superior D'Enginyers de Camins, Canals I Ports. Universitat Politècnica de Catalunya, Barcelona, España.

Rots, J. G. (1997). *Structural masonry: An experimental/numerical basis for practical design rules*. AA Balkema.

Rots, J. G. and De Borst, R. (1987). "Analysis of mixed-mode fracture in concrete." *Journal of engineering mechanics*, 113(11), 1739–1758.

Simo, J. and Hughes, T. (1998). *Computational inelasticity*, Vol. 7 of *Interdisciplinary applied mathematics*. Springer.

Simo, J. and Ju, J. (1987). "Strain-and stress-based continuum damage models ii. computational aspects." *International journal of solids and structures*, 23(7), 841–869.

Simo, J. and Ju, J. (1989). "Strain-and stress-based continuum damage models i. formulation." *Mathematical and Computer Modelling*, 12(3), 378.

Tao, X. and Phillips, D. V. (2005). "A simplified isotropic damage model for concrete under bi-axial stress states." *Cement and Concrete Composites*, 27(6),

716–726.

Truesdell, C. and Toupin, R. (1960). *The classical field theories*. Springer.

Turkstra, C. (1970). "Resistencia de muros de mampostería ante cargas verticales excéntricas." *Instituto de Ingenieria, Universidad Nacional Autonoma de Mexico*.

Vargas-Félix, M. and Botello-Rionda, S. (2012). "FEMT, an open source library and tools for solving large systems of equations in parallel.

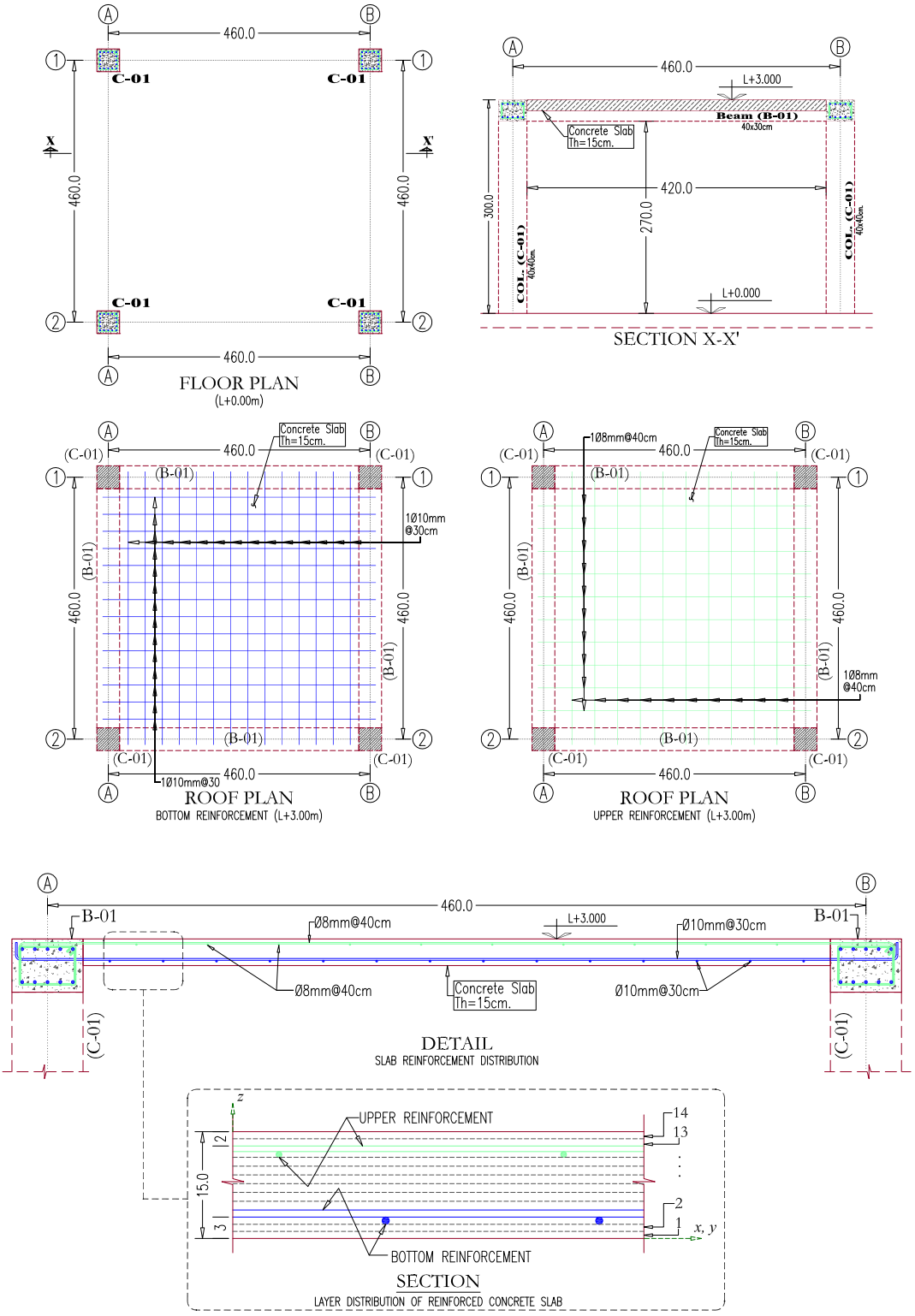

FIG. 1. Structural drawings (plans and elevations) of a typical framing construction.

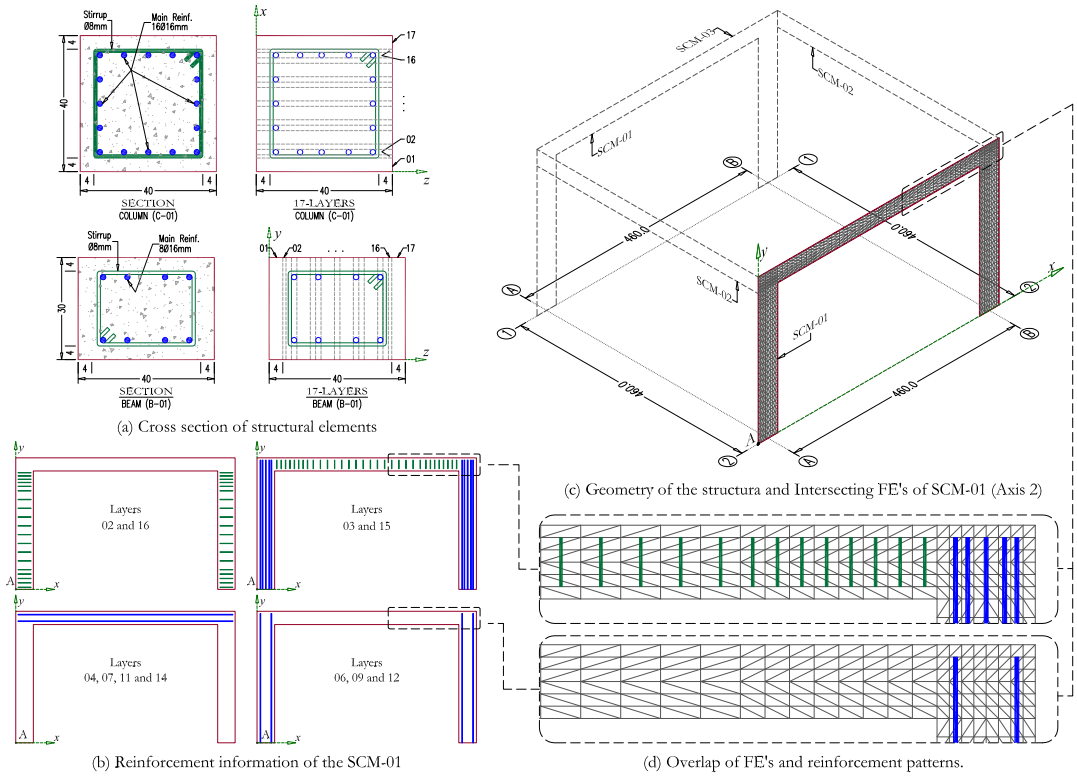

FIG. 2. Boundaries of *SCM* with their FE and steel reinforcement patterns.

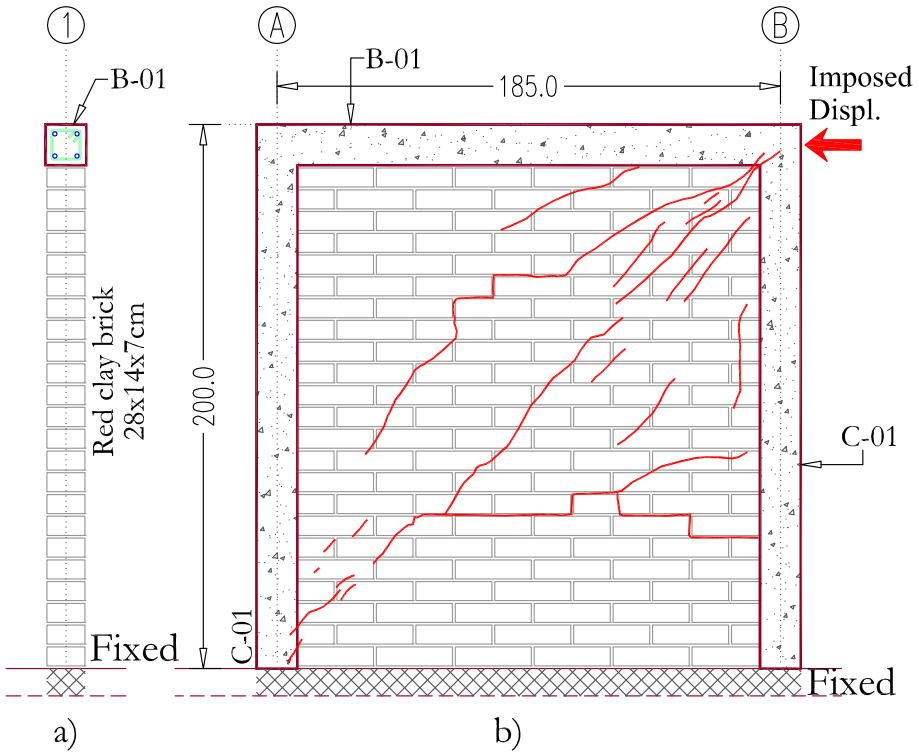

FIG. 3. Geometry, crack patterns, loading and boundary conditions for cantilever wall with masonry in-fill

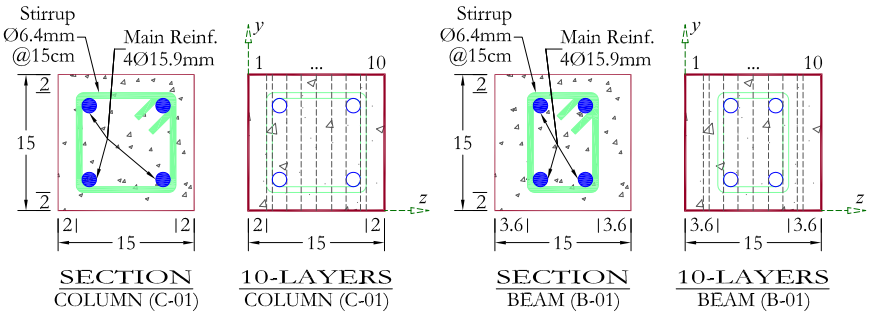

(a) Cross sections of structural elements

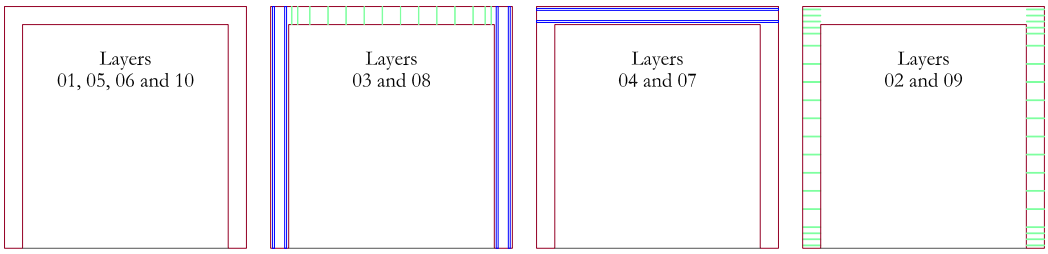

(b) Distribution of steel reinforced fibers within layers

FIG. 4. Distribution of reinforced fibers, and cross section of structural elements for a reinforced concrete frame with masonry in-fills.

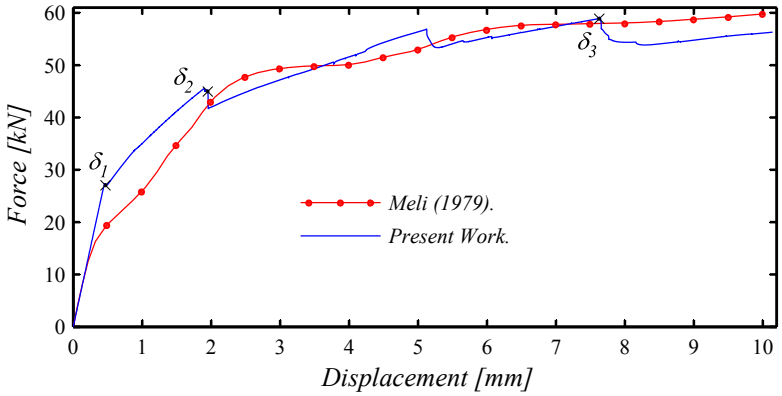

(a) Load-displacement comparison.

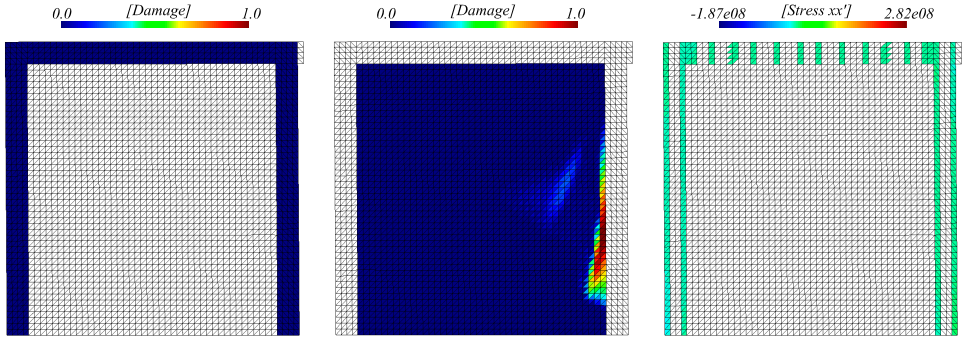

(b) Imposed displacement δ_1= 0.46mm

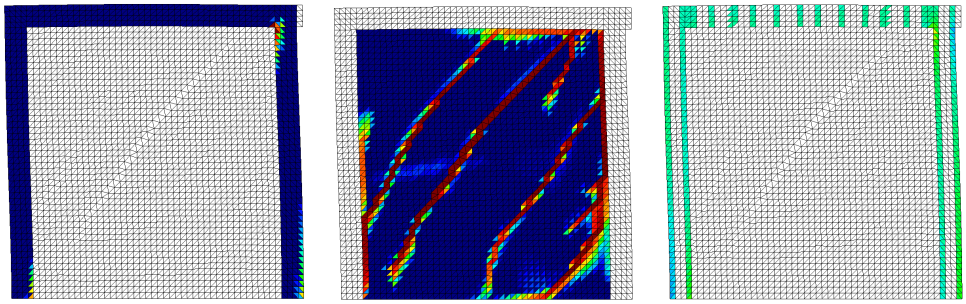

(c) Imposed displacement δ_2= 1.94mm

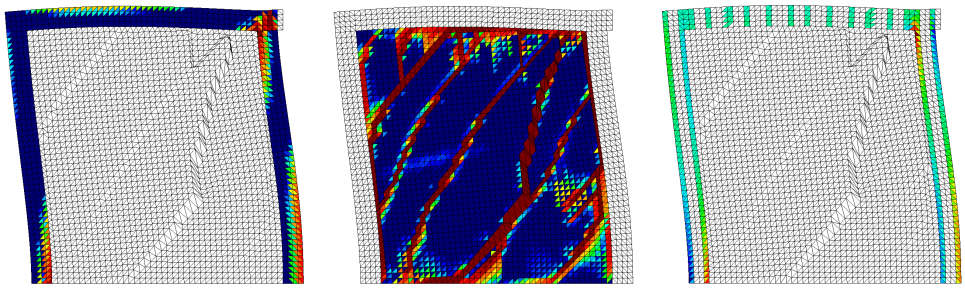

(d) Imposed displacement δ_3= 7.66mm

FIG. 5. Numerical results for a reinforced concrete frame with a masonry in-fill.

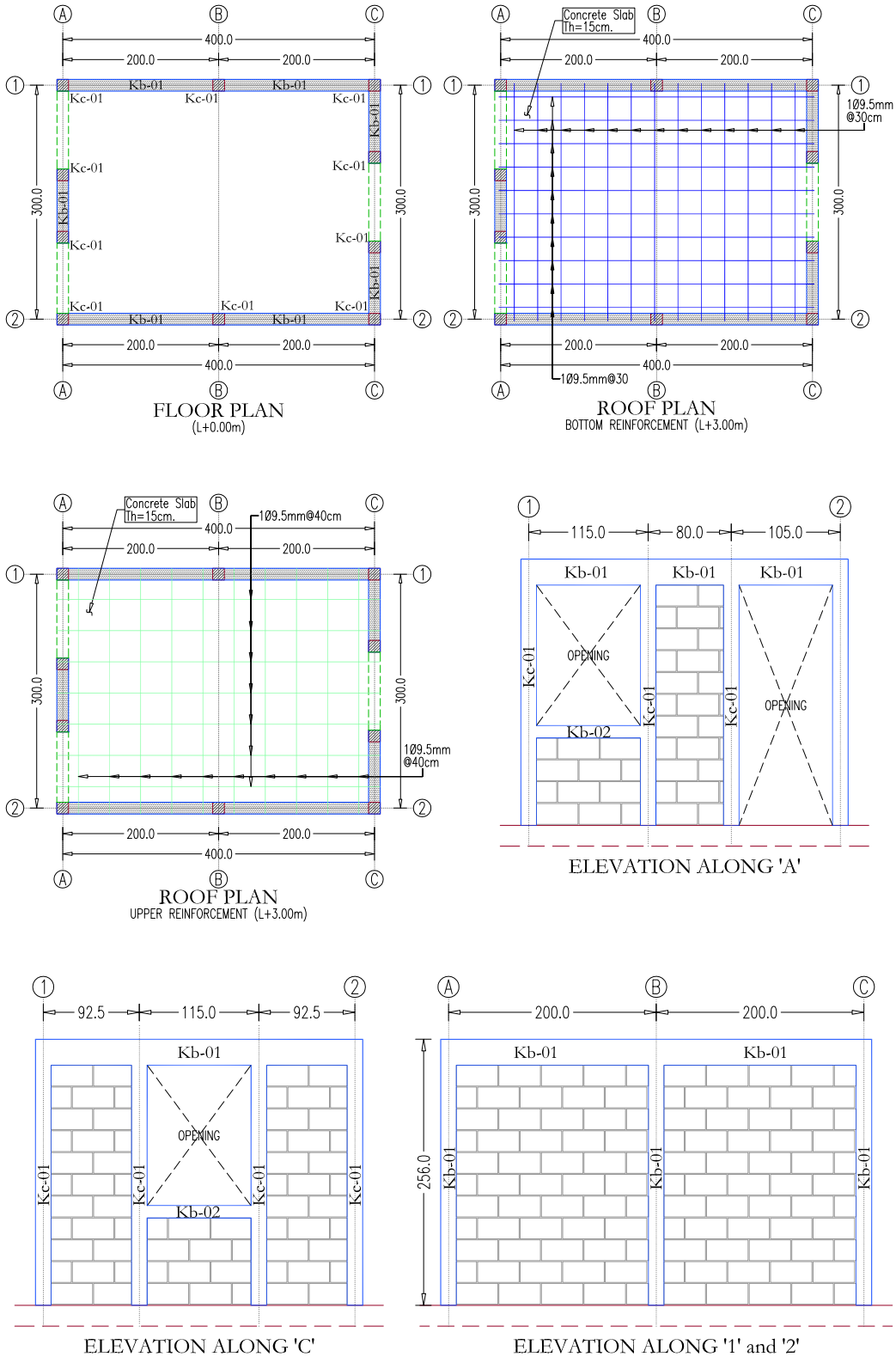

FIG. 6. Structural Drawings - One storey construction (units: cm).

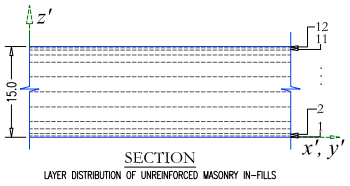

(a) Detailed section (units: cm)

1	2	3	4	5	6
2.0	4.0	8.0	12.0	24.0	25.0
7	8	9	10	11	12
25.0	24.0	12.0	8.0	4.0	2.0

(b) Layer distribution (units: mm)

FIG. 7. Detailed section of masonry in-fills.

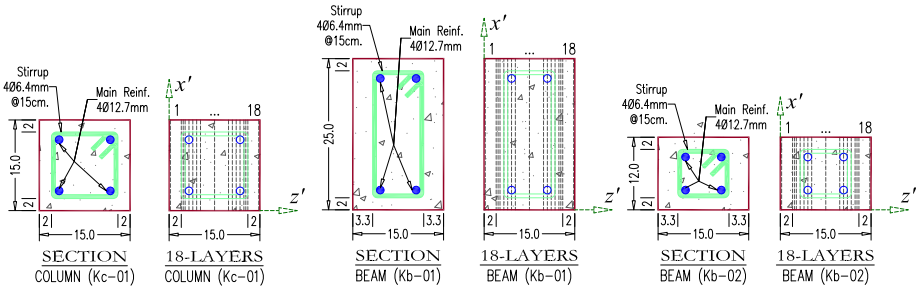

(a) Detailed section (units: cm)

1	2	3	4	5	6	7	8	9
2.0	18.0	3.20	3.20	6.35	6.35	6.35	6.35	23.20
10	11	12	13	14	15	16	17	18
23.20	6.35	6.35	6.35	6.35	3.20	3.20	18.0	2.0

(b) Layer distribution (units: mm)

FIG. 8. Detailed section of columns and beams.

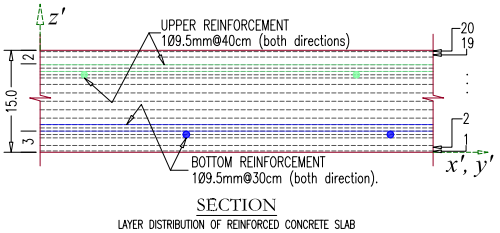

(a) Detailed section (units: cm)

1	2	3	4	5	6	7	8	9	10
2.0	8.0	11.2	5.0	5.0	4.75	4.75	9.5	12.4	12.4
11	12	13	14	15	16	17	18	19	20
12.4	12.4	9.5	4.75	4.75	5.0	5.0	11.2	8.0	2.0

(b) Layer distribution (units: mm)

FIG. 9. Detailed section of slab.

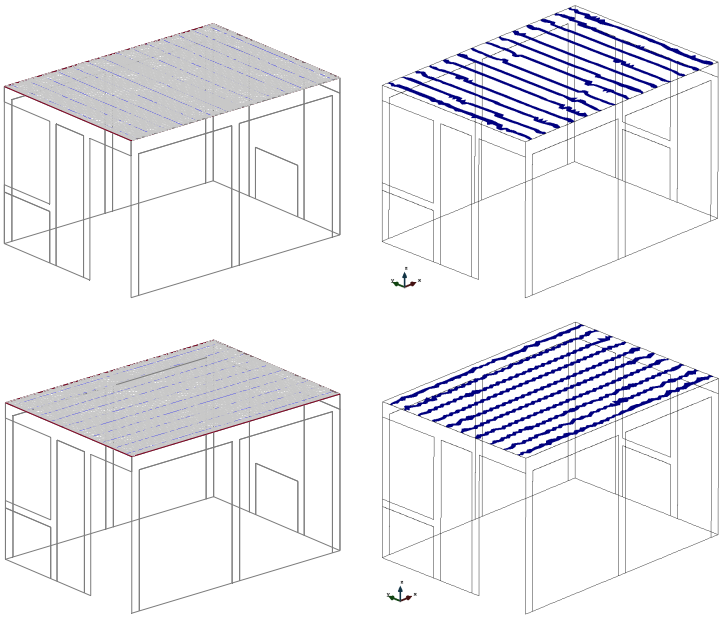

FIG. 10. Fibers reinforcement on slab.

MASONRY BEARING WALL

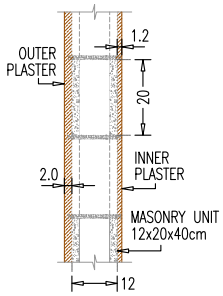

MATERIAL	THICKNESS (cm)	WEIGHT (kg/m^3)	WEIGHT (kg/m^2)
MASONRY WALL	12.0	1500	180
INNER PLASTER	1.2	1500	18
OUTER PLASTER	2.0	2100	42
DEAD LOAD*	DUE TO CONCRETE		--
	DUE TO MORTAR		20

$D_L = 260\ kg/m^2$

ROOFING SYSTEM

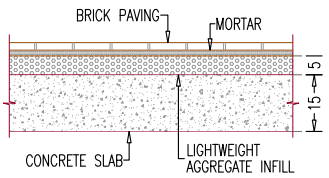

MATERIAL	THICKNESS (cm)	WEIGHT (kg/m^3)	WEIGHT (kg/m^2)
BRICK PAVING	2.0	1500	30
MORTAR	1.50	2100	31.5
AGGREGATE	5.0	1200	60
CONRETE SLAB	15.0	2400	360
DEAD LOAD*	DUE TO CONCRETE		20
	DUE TO MORTAR		20

$D_L = 521.5\ kg/m^2$

FIG. 11. Dead loads - masonry bearing walls and roofing system.

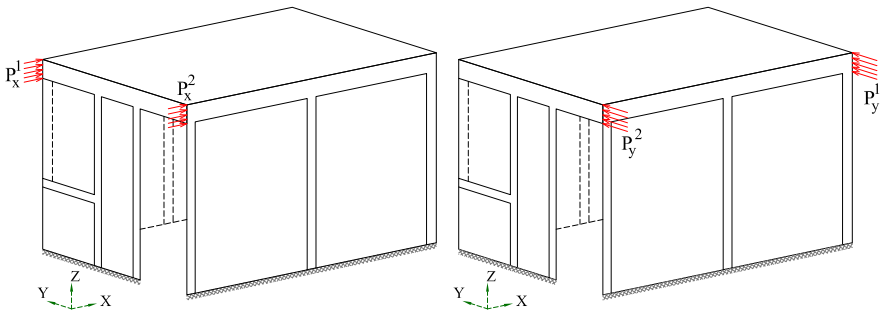

FIG. 12. Application loads on pushover analysis.

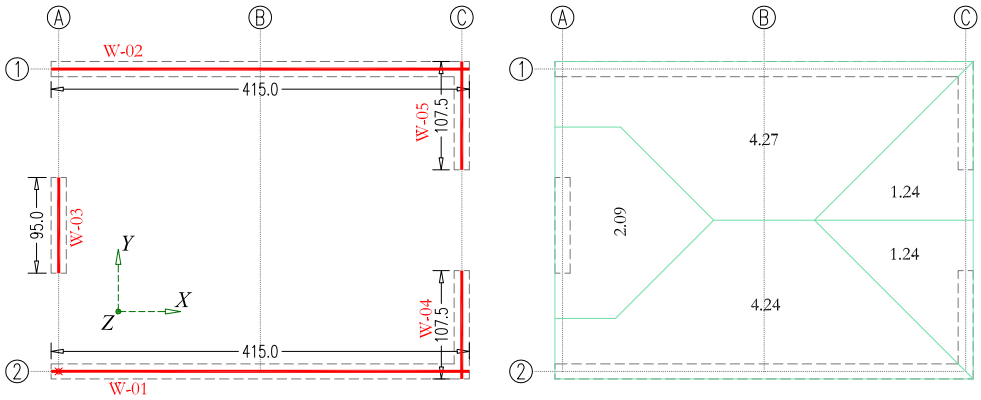

FIG. 13. Bearing walls and tributary areas (units: cm).

Wall Number	W-01	W-02	W-03	W-04	W-05
Stiffness(kN/m)	474002.72	474002.72	14787.67	20907.57	20907.57
Shear Strength (kN)	221.53	221.59	52.77	57.65	57.65

TABLE 1. Stiffness and shear strength of masonry walls.

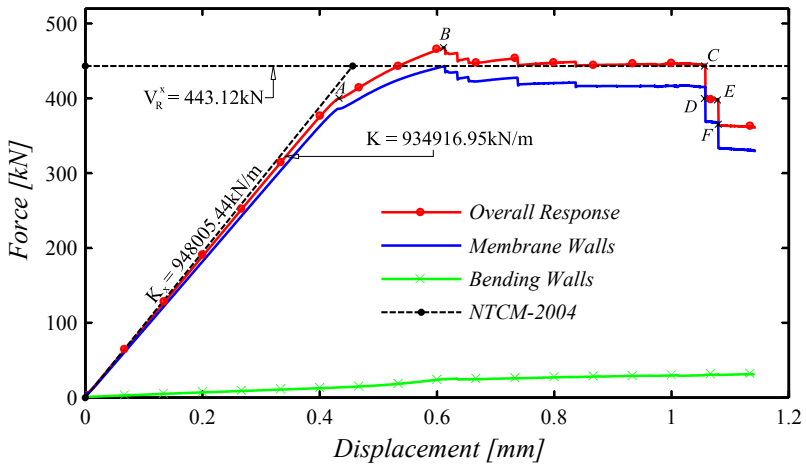

FIG. 14. Displacement-force response of model B-OSC in X direction.

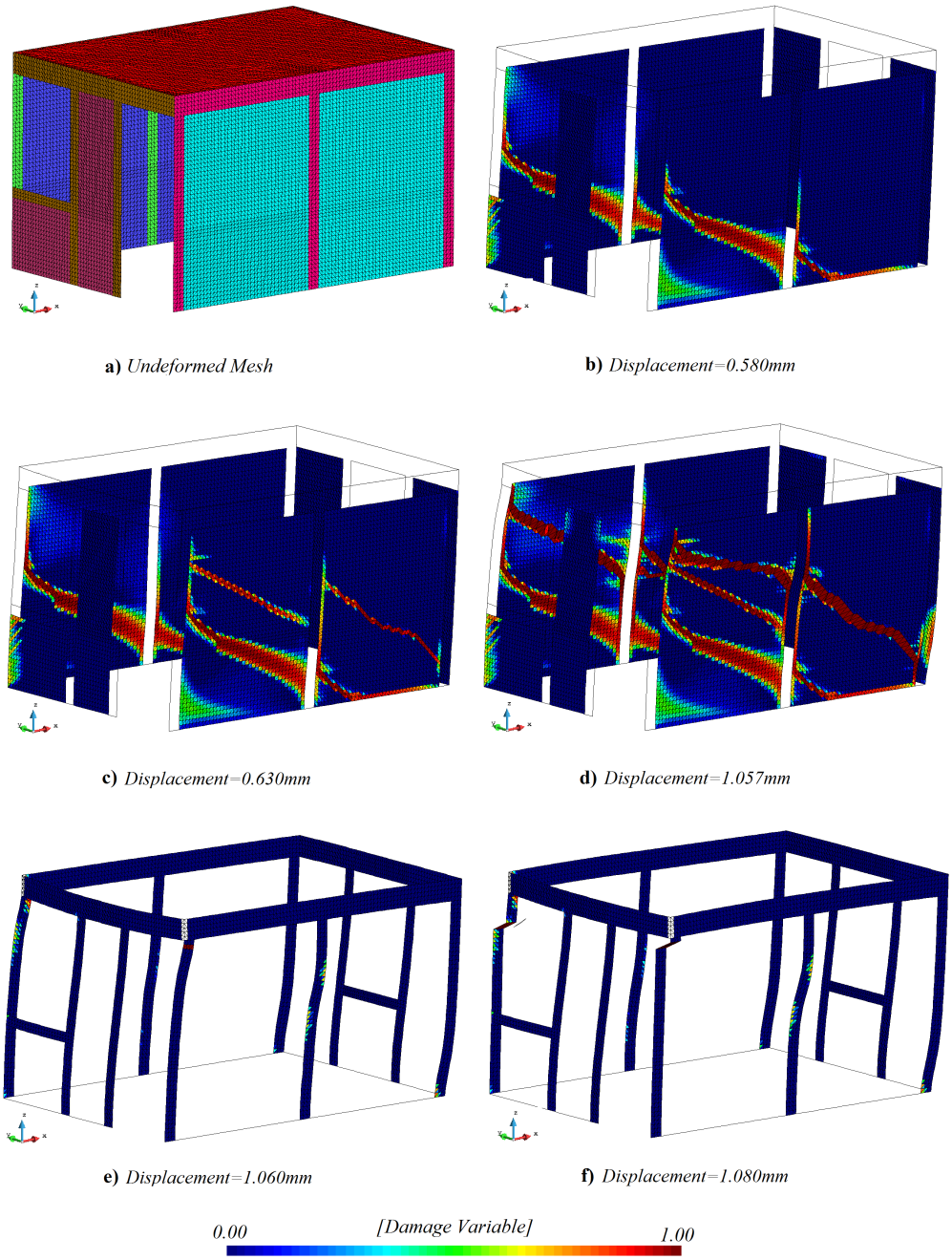

FIG. 15. Front isometric view - Damage evolution of masonry walls in X direction.

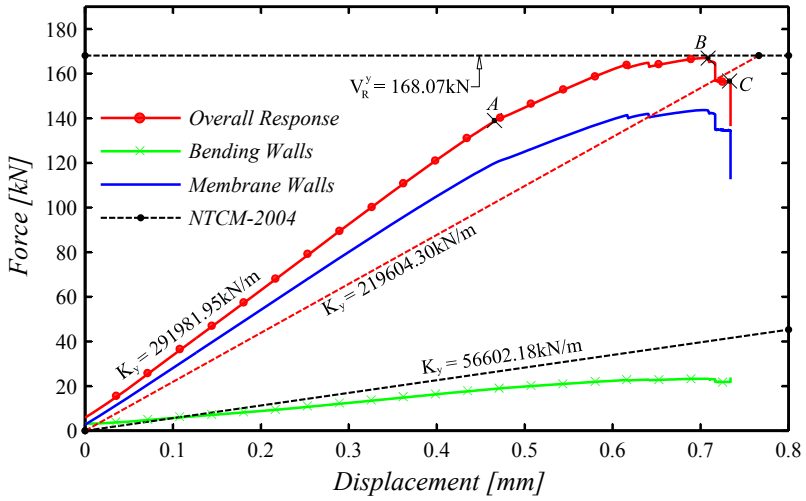

FIG. 16. Displacement-force response of model B-OSC in Y direction.

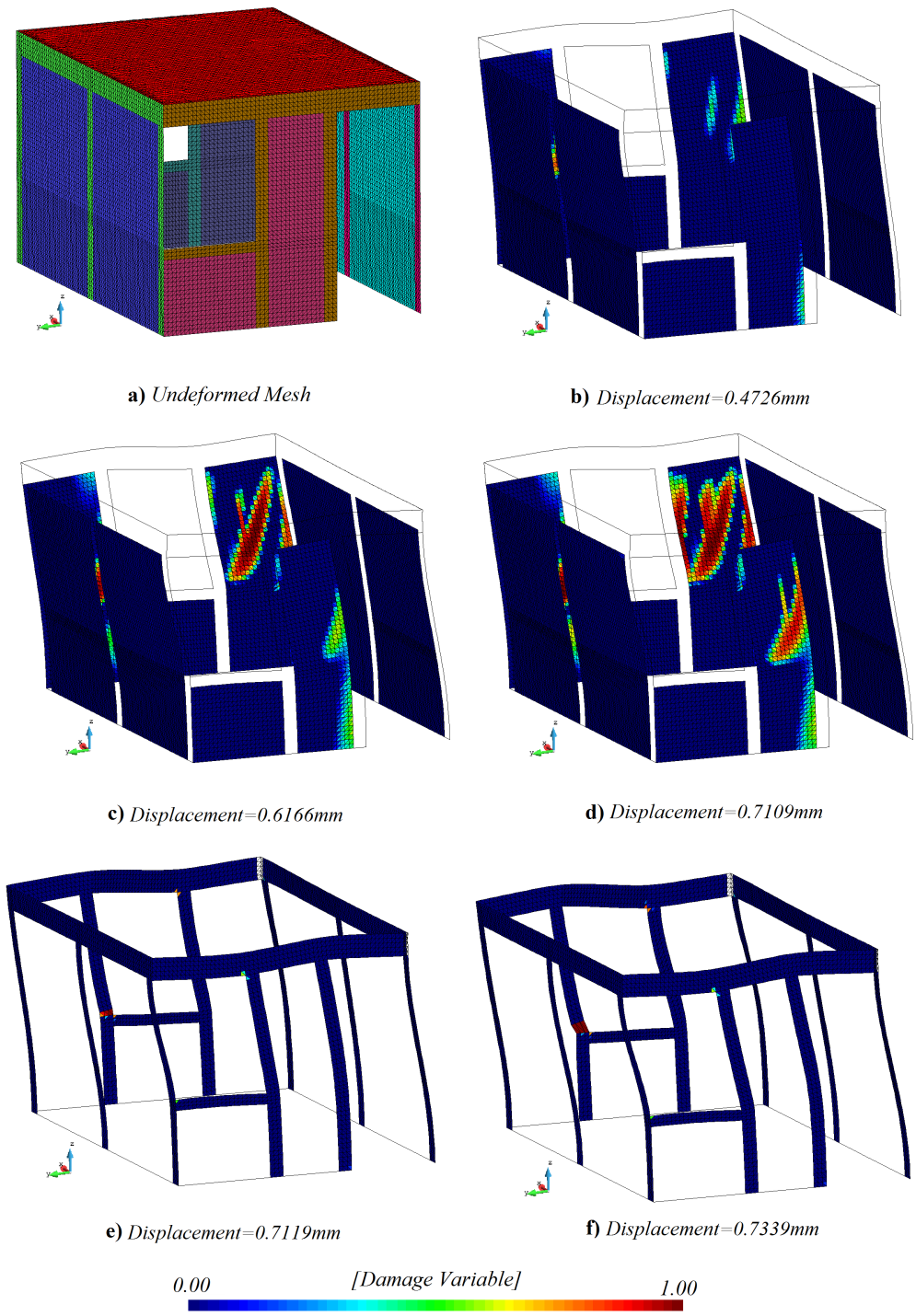

FIG. 17. Front isometric view - Damage evolution of masonry walls in Y direction.